A Mercury surface radiometric model for SIMBIO-SYS instrument suite on board of BepiColombo mission

Slemer, A., Zusi, M., Simioni, E., Da Deppo, V., Re, C., et al.

A. Slemer, M. Zusi, E. Simioni, V. Da Deppo, C. Re, V. Della Corte, G. Filacchione, P. Palumbo, F. Capaccioni, G. Cremonese, "A Mercury surface radiometric model for SIMBIO-SYS instrument suite on board of BepiColombo mission," Proc. SPIE 10698, Space Telescopes and Instrumentation 2018: Optical, Infrared, and Millimeter Wave, 106984C (6 July 2018); doi: 10.1117/12.2314836

SPIE.

Event: SPIE Astronomical Telescopes + Instrumentation, 2018, Austin, Texas, United States

A Mercury surface radiometric model for SIMBIO-SYS instrument suite on board of BepiColombo mission

A. Slemer[a], M. Zusi[b], E. Simioni[c], V. Da Deppo[a,c], C. Re[c], V. Della Corte[b,d], G. Filacchione[b], P. Palumbo[b,d], F. Capaccioni[b], and G. Cremonese[c]

[a]CNR-IFN Padova, Via Trasea 7, 35131 Padova, Italy
[b]INAF-IAPS, Via Fosso del Cavaliere 100, 00133 Roma, Italy
[c]INAF-OAPD, Vicolo dell'Osservatorio 5, 35122 Padova, Italy
[d]Dipartimento di Scienze e Tecnologie (DIST), Università degli Studi di Napoli Parthenope, Centro direzionale di Napoli Isola C4, 80143 Napoli

ABSTRACT

The BepiColombo mission represents the cornerstone n.5 of the European Space Agency (ESA) and it is composed of two satellites: the Mercury Planetary Orbiter (MPO) realized by ESA and the Mercury Magnetospheric Orbiter (MMO) provided by the Japan Aerospace Exploration Agency (JAXA). The payload of the MPO is composed by 11 instruments. About half of the entire MPO data volume will be provided by the "Spectrometer and Imagers for MPO BepiColombo Integrated Observatory System" (SIMBIO-SYS) instrument suite.

The SIMBIO-SYS suite includes three imaging systems, two with stereo and high spatial resolution capabilities, which are the Stereoscopic Imaging Channel (STC) and High Resolution Imaging Channel (HRIC), and a hyper-spectral imager in the Vis-NIR range, named Visible and near Infrared Hyper-spectral Imager (VIHI).

In order to test and predict the instrument performances, a radiometric model is needed. It consists in a tool that permits to know what fraction of the incoming light is measured by the detector. The obtained signal depends on the detector properties (such as quantum efficiency and dark current) and the instrument transmission characteristics (transmission of lenses and filter strips, mirrors reflectivity).

The radiometric model allows to correlate the radiance of the source and the signal measured by each instrument. We used the Hapke model to obtain the Mercury reflectance, and we included it in the radiometric model applied to the STC, HRIC and VIHI channels. The radiometric model here presented is a useful tool to predict the instruments performance: it permits to calculate the expected optical response of the instrument (the position in latitude and longitude of the filter footprints, the on-ground px dimensions, the on-ground speed, the smearing and the illumination angles of the observed points), and the detector behavior (the expected signal and the integration time to reach a specific SNR).

In this work we derive the input flux and the integration times for the three channels of SIMBIO-SYS, using the radiometric model to obtain the source radiance for each Mercury surface area observed.

Keywords: SIMBIO-SYS, Radiometric model, Mercury, Hapke, reflectance

1. INTRODUCTION

The cornerstone Bepicolombo is an interdisciplinary mission realized through a partnership between the European Space Agency (ESA) and the Japan Aerospace Exploration Agency (JAXA) to explore the planet Mercury.[1] Two spacecrafts, i.e. the Mercury Planetary Orbiter (MPO) and the Mercury Magnetospheric Orbiter (MMO), will investigate the entire planet and its environment for nearly 2 years (1 year nominal mission plus 1 year of extended mission) starting from 2026. The MPO satellite follows an elliptical orbit around the Mercury planet; the orbit eccentricity is 0.1486 and the semi-major axis 3430 km. The argument of the periherm is 16° and the altitude at periherm is 480 km at the beginning of the mission. During the entire mission the periherm argument

alessandra.slemer@pd.ifn.cnr.it

Space Telescopes and Instrumentation 2018: Optical, Infrared, and Millimeter Wave, edited by Makenzie Lystrup, Howard A. MacEwen, Giovanni G. Fazio, Proc. of SPIE Vol. 10698, 106984C
 · doi: 10.1117/12.2314836

and the minimumm S/C altitude decrease. The planet Mercury follows an orbit around the Sun with eccentricity e=0.205632 and semi-major axis a=0.387098 AU.

A crucial role in the analysis in the geological and mineralogical investigation of Mercury surface will come from the Spectrometer and Imagers for MPO BepiColombo-Integrated Observatory SYStem Suite (SIMBIO-SYS). SIMBIO-SYS includes two imaging systems with stereo and high spatial resolution capabilities, which are the Stereoscopic imaging Channel (STC) and High Resolution Imaging Channel (HRIC), and a hyperspectral imager in the Vis-NIR range, named Visible and near Infrared Hyperspectral Imager (VIHI). STC will perform 55-120 m spatial resolution global mapping in stereo resolution and tergeting with color filters, HRIC is a camera for the high resolution imaging (6-12 m/px) in panchromatic and broad-band filters, and VIHI will perform spectral global mapping of the Mercury surface in the 400-2000 nm spectral range. The instrument has been designed with the goal of maximizing the scientific return and minimizing the resource requirement, primarly mass and power. The main scientific goal of SIMBIO-SYS is to map the Mercury surface in different wavelengths and with different spatial resolutions to investigate the morphology and mineralogical composition of the planet surface.

The paper is structured as follows. Firstly we shortly describe the SIMBIO-SYS instrument (section 2), then the pipeline of the radiometric model is given (section 3), and finally we show the preliminary outputs obtained applying the radiometric model (section 4).

2. BASICS OF SIMBIO-SYS INSTRUMENT

Table 1. Optical characteristics and scientific requirements of STC. Scientific requirements are defined considering panchromatic filter at periherm of the first orbit (480 km).

Optical characteristics		**Scientific requirements (Global Mapping)**	
Optical concept	Catadrioptic: off-axis portion of a modified Schmidt telescope with folding mirror fore-optics	Scale factor (along-track x cross track)	61.2x55.1 m/px
Stereo solution	Two optical channel with common detector and most of the optical elements	Swath (along track x cross track)	23.5x4.9 km
Focal length	95.2 mm	Stereoscopic properties	$\pm 21.375°$ bore-sight angle vs nadir
Pupil size	15 mm	Vertical accuracy	80 m
IFOV	105 μrad	**Scientific requirements(All filters)**	
Focal ratio	f/6.3	Fraction of diffraction encircled energy (EE)	$> 70\%$ inside 1 pixel
Distortion	$< 1.6\%$	Diffraction modulation transfer function (MTF)	$> 60\%$ at Nyquist Frequency
FoV (cross track)	5.38°	Wavelength coverage	410-930 nm (6 filters)
FoV (along track)	2.4° for panchromatic and 0.38° for color filters	Filters	PAN (700 ± 100 nm) F420 (420 ± 10 nm) F550 (550 ± 10 nm) F750 (750 ± 10 nm) F920 (920 ± 10 nm)

The SIMBIO-SYS instrument is based on three different channels with a common Main Electronics (ME) and power supply. Each channel is composed by its optics, detector, thermal hardware, proximity electronics and interface for power supply. The measurements strategy is based on the coordinated operations of the three channels of SIMBIO-SYS.

While the HRIC and VIHI channels observations will be done during the entire Mercury-year, for STC the observations are constrained in the true anomaly interval $138° \leq \nu \leq 222°$. The constraints for the observations are due to the different characteristics of the three channels, which are briefly described below.

2.1 The STC channel

STC is a double wide angle camera designed to image specific portions of the Mercury surface from two different perspectives, providing a panchromatic stereo images pair required for the Digital Terrain Model (DTM) generation,[2],[3] and color images with broad band filters. Furthermore, it will implement a new stereo acquisition concept based on the push-frame[4]

The design of the camera consists in two sub-channels that are looking at two different directions (±20° with respect to the nadir) on the Mercury surface. The two incoming beams are deflected and focalized on one common detector. The characteristics of the STC optical design and the scientific requirements are summarized in table 2.[5] For each sub-channel, STC can acquire simultaneously three quasi-contiguous areas of the Mercury surface in different colors. The useful FoV is divided in three portions that correspond to the filters of the channel considered (5.38°x2.4° for panchromatic filter, and 5.38°x0.4° for color filters). The detector of STC is a 2048 x 2048 hybrid Si-PIN based on CMOS technology, back-illuminated with 10 μm of pixel size.[6] The choice of a CMOS instead of a CCD detector is due to the CMOS better tolerance to radiations and to the need of integrated then read (ITR) acquisition, which allows to avoid a mechanical shutter.

2.2 The HRIC channel

The SIMBIO-SYS High Resolution Imaging Chanel (HRIC) is a visible imaging camera characterized by the high ground pixel resolution, which is estimated $\sim$ 6m/px at 480 km from the planet surface. This feature allows to analyze the details of target areas of Mercury surface.

HRIC is a catadioptric telescope with a focal length of 800 mm. The optical design is based on a classic Ritchey-Chretien configuration modified with a dedicated refractive field corrector, to compensate for the field of view dependent aberrations. This configuration gives a pixel resolution of 2.6" for a pixel size of 10 μm. The focal ratio of the instrument is F/8.9, which allows to have diffraction limited performance for a wavelength of 400 nm. The 2.6" IFoV per px guarantees, together with the 2048x2048 detector, a squared FOV of 1.47°. The catadrioptric solution is more convenient than a pure reflective solution because it gives a good balance of the aberations, thus guaranting to reach the required optical performance all over the FoV.

The detector is a hybrid 2048x2048 Si-PIN CMOS, back illuminated with 10 μm of pixel size. The CMOS detector type used for HRIC is the same of STC. Four filters are placed over the detector: a panchromatic filter (centered at 650 nm and with 400 nm of bandwidth), and three broad band filters (centered at 550, 750 and 880 nm, with 40 nm of bandwidth) in order to investigate the surface local geo-mineralogical characteristics.

Table 2. HRIC optical parameters.

Parameters	**Values**
Aperture (diameter)	90 mm
Focal length	800 mm
f/number	8.9
FOV	1.47°
pixel IFOV	12.5μmrad
central obscuration	10 % diameter
Spectral range	400-900 nm
Spectral bands	Panchromatic (650 nm), 550nm, 750nm, 880nm

2.3 The VIHI channel

The Visibile and Infrared Hyperspectral Imager (VIHI) is the spectral channel of the SIMBIO-SYS optical payload. The instrument consists in a modified Schmidt telescope joined to a Littrow spectrometer with a flat grating.

The focal plane is an MCT 256x256 array, with a pixel pitch of 40x40 μm and a full-well of 2 Me^-. The focal plane packaging also includes an order sorting filter, a zero order light trap, a cold shield to reject parasitic light and an active thermo-cooler (TEC), which stabilizes the detector at the nominal operating temperature of T=220 K. The VIHI channel operates in $0.4 - 2.0\,\mu$m wavelength range with 256 spectral bands. The spectral sampling is 6.25 nm/band and the FOV width is 64 mrad, with 256 spatial pixels each having a 250 μrad Instantaneous Field of View (IFOV). The instrument operates in push-broom mode with a maximum resolution of 100 m/px (relative to an MPO altitude of 400 km).

The main VIHI optical parameters are summarized in Table 2.3.

Table 3. VIHI optical parameters

Parameters	**Values**
Aperture	25 mm
Focal length	160 mm
f/number	64
FOV	64.0x0.25 mrad
IFOV	0.25x0.25 mrad
Scale	100 m/px from 400 km
Spatial samples	256
Spectral bands	256
Spectral dispersion	6.25 nm/band

3. APPLICATION OF THE MERCURY RADIOMETRIC MODEL TO SIMBIO-SYS CHANNELS

The value of the flux detected by the SIMBIO-SYS instrument depends both on the source properties (spectral radiance), and the instrument characteristics, which vary with the channel considered.

The radiometric model here derived is a tool that give the estimation of the expected signal detected by the instrument, given the position of the spacecraft with respect to the target and the source. The radiance of the source depends on the properties of the light source and on those of the considered surface, which are expressed by the reflectance. We derive the radiometric model of the Mercury surface taking into account the Hapke's reflectance model[7–10] with parameters derived by Domingue.[11]

The expression and parameters of this model account for surface roughness, porosity, grain scattering properties, and both the mechanism proposed to create the opposition surge,[12] and the incidence (i), emission (e) and phase (α) angles. In this work we consider the Matabei dataset derived by Domingue.[11] This dataset has been obtained from the images acquired during MESSENGER orbital operations prior to 24 May 2011 [4]. The coherent back-scatter opposition parameters are set to the values $b_c = 2.3$ and $h_c = 0.075$, while the shadow hiding opposition parameter (b_s) is set to zero.[11,12] We use a quadratic interpolation to obtain the values of these parameters for all the wavelengths between 300 nm and 1100 nm, obtaining a series of functions (one for each parameter) that are included in the reflectance equation. The result is a reflectance function for all the wavelengths in the visible range that depends on incidence, emission and phase angles, and thus it depends on the surface point observed.

Figure 1 shows the flowchart of the radiometric model described in this work. It receives as inputs: the reference time, the position of Mercury with respect to the Sun (the true anomaly ν) and the instrument

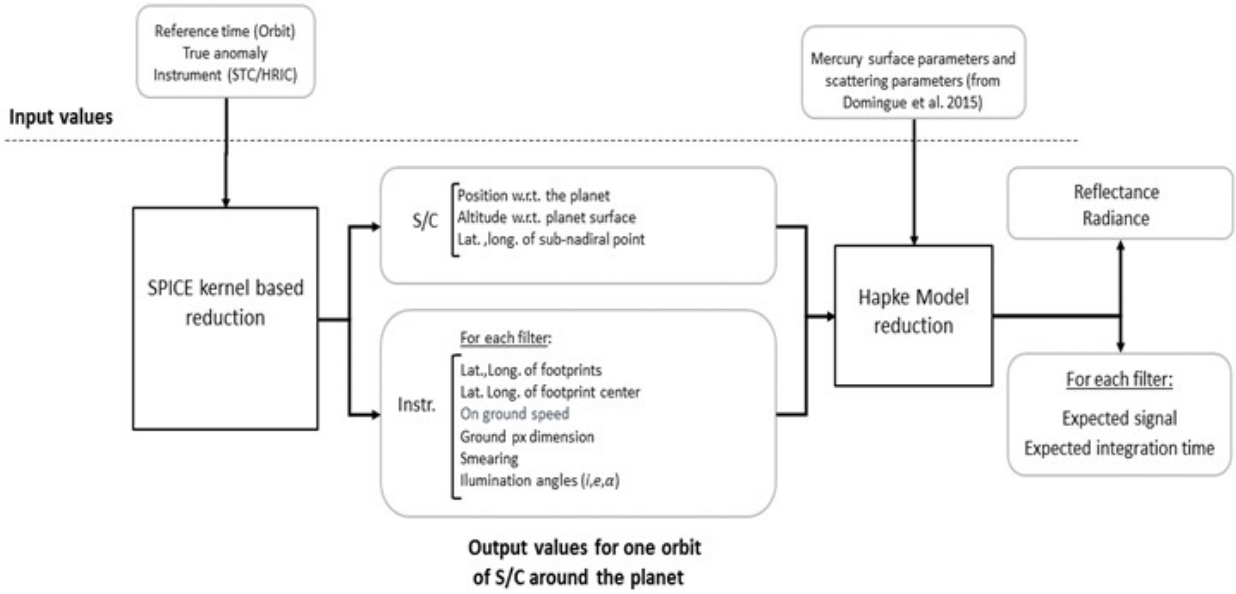

Figure 1. Flowchart of the radiometric model developed

considered. The SPICE tools for the BepiColombo mission have been implemented to retrieve output data. The outputs of the radiometric model can be divided in three sections:

- The outputs related to spacecraft and instrument (in Figure 1 the two boxes at the center of the image) which include both the general information about the spacecraft and the geometrical information for each filter
- The radiometric data including the planet reflectance, the radiance and the expected signal at the detector.
- The performance outputs are: the best expected integration time to avoid the detector saturation level, the expected dark current and the so called 'smearing time', which is the time due to the specefract to cover the distance equal to the dimension of the on-ground px and it is the maximum acceptable integration time to avoid image. The value for the smearing time considered for STC is the time corresponding to a boresigth movement of 1/4 px.

When the input source radiance is defined, the signal measured by the detector can be determined. It is interesting to obtain these quantities for a series of scenarios in which the true anomaly of Mercury and the position of the S/C around the planet change. The scenarios here considered are the most representative of the conditions that will take place during the BepiColombo mission.

The signal at the entrance of the optical system consists of the thermal radiation of the planet (the black body at the planet surface temperature) and the contribution of the Sun radiation reflected by the surface of Mercury. For the three SIMBIO-SYS channels, the weavelength corresponding to the maximum thermal radiation is out of each sub-channel spectral range. For this reason, the radiation due to planet itself is considered negligible.

The spectral radiant flux $\phi(\lambda)$[W/nm], which enters the instrument, can be expressed as:

$$\phi(\lambda) = I(\lambda, \nu) \cdot A \tag{1}$$

where I(λ) is the spectral irradiance of the source and A is the entrance pupil area [A $= \pi \cdot (\mathrm{D}/2)^2$] with D as the pupil diameter. The spectral irradiance derives from the equation:

$$I(\lambda, \nu) = B_{\odot} \cdot \pi \left(\frac{R_{\odot}}{r} \right)^2 \cdot R(i, e, \alpha) \cdot \Omega \tag{2}$$

where $B_{\odot} \cdot \pi \left(\frac{R_{\odot}}{r}\right)^2$ is the fraction of the Sun spectrum that illuminate the Mercury surface and Ω is the solid angle subtended by the considered imaged area. Usually the solid angle considered is the one subtended by one pixel ($\Omega_{px} = (\text{pxscale})^2$). The term $R(i, e, \alpha)$ is the Mercury surface reflectance, which depends on the incident (i), emission (e) and phase (α) angles. The Reflectance as a function of the weavelength has been obtained by using the Hapke reflectance model,[9,10] with parameters obtained by Domingue.[12]

The flux that reaches the detector, measured in $[W/nm]$, is reduced by the optics ($T(\lambda)$) and by the filter transmission ($F(\lambda)$):

$$\phi_{det}(\lambda) = \phi(\lambda) \cdot T(\lambda) \cdot F(\lambda) \tag{3}$$

The detector collects part of the incident photons, those that are interacting with its substrate following the quantum efficiency ($QE(\lambda)$), and it registers the signal in electrons. Therefore, the incoming flux has to be divided by the photon energy (hc/λ) in order to obtain the number of incident photons. Then it is multiplied for the QE to obtain the number of interacting photons and thus the flux in $[e^-/(nm \cdot ms)]$:

$$\phi_e(\lambda) = \phi_{det}(\lambda) \cdot \left(\frac{\lambda}{hc}\right) \cdot QE(\lambda) \tag{4}$$

The flux expressed in number of electrons per ms is:

$$F_e = \int_{\Delta\lambda} \phi_e(\lambda) \cdot d\lambda \tag{5}$$

where $\Delta\lambda$ is the bandwidth of each filter.

The final flux is converted in DN/ms dividing the F_e by the Inverse Gain (IG), which is the number of electron per DN. For the STC and HRIC detector the IG is $7e^-/DN$,[5] while for VIHI is $\sim 150e^-/DN$ The flux in DN/ms is:

$$F = \frac{S_e}{IG} = \frac{A}{IG \cdot hc} \int_{\Delta\lambda} I(\lambda) \cdot T(\lambda) \cdot F(\lambda) \cdot QE(\lambda) \cdot \lambda \cdot d\lambda = \frac{1}{IG} \int_{\Delta\lambda} I(\lambda) \cdot ITF(\lambda) \cdot \lambda \cdot d\lambda \tag{6}$$

Where the ITF is the Instrument Transfer Function.

The goal of the radiometric model for the SIMBIO-SYS instruments is to convert the radiance of the target (expressed in physical units) in the signal measured by the detector (in DN/ms) . The value detected depends both on the source properties (spectral radiance) and the instrument characteristics, which change with the channel considered.

4. OUTPUTS OF THE RADIOMETRIC MODEL

Using the SPICE kernels available for the BepiColombo mission we derive some useful information concerning the MPO orbit around Mercury. Figure 2 shows the S/C altitude (left side panel) and the velocity of the S/C and its ground projection (right side panel) obtained for the time interval that describes the half of the orbit that corresponds to the illuminated part of the planet. The x-axis indicates the relative time with respect to the instant that corresponds to the periherm.The upper x-axis shows the latitude of the subnadiral point, which is the intersection between the line normal to the surface that contains the S/C and the surface plane. Both plots refer to an orbit in which Mercury is at the aphelion.

Figure 2 allows us to make some considerations about the spacecraft orbit. Firstly, since the line of apsis of the MPO orbit is tilted with respect to the equatorial plane of the planet, the minimum distance between the MPO and the Mercury ground surface is reached for non zero sub-nadiral latitude. Furthermore, the on ground resolution of the SIMBIO-SYS instrument depends on the MPO altitude with respect to the ground, so that the maximum resolution of SIMBIO-SYS instruments can be reached when the MPO is over the 16° north-latitude. This is true for the first orbit of MPO, because during the entire mission the argument of the periherm changes.

In this section we briefly show some of the output that can be obtained by applying the radiometric model to the different instruments, which can be useful to study the instruments performance and to plan the observation strategy.

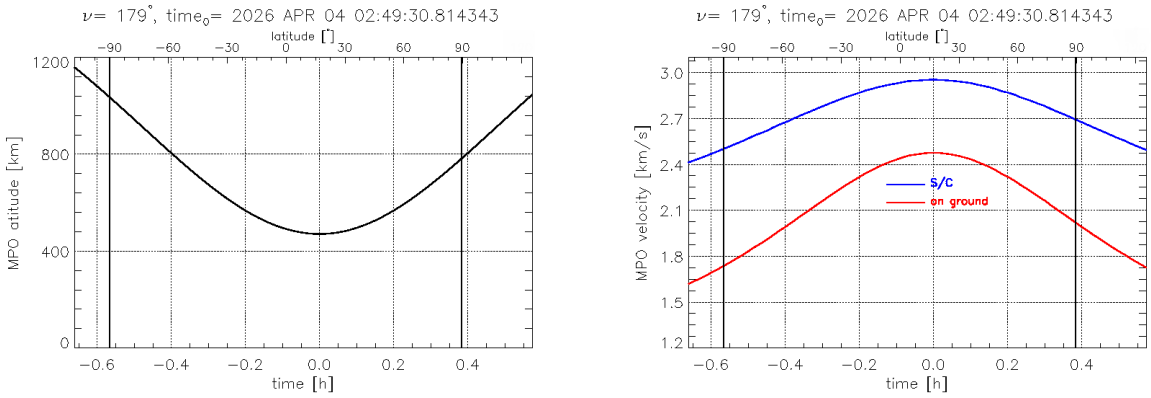

Figure 2. Some of the outputs that describe the spacecraft orbit around Mercury: the left side panel shows the S/C altitude w.r.t the ground, while the right side panel represents the S/C velocity and the subnadiral velocity. The x coordinate represents the time relative to those of the periherm ($time_0$), while the upper x-axis shows the subnadiral latitude. All plots refer to an orbit of the S/C for which Mercury is at aphelion.

4.1 Expected signal and integration time

Once the Mercury surface radiance for each observed area is known, we can calculate the expected signal measured by the detector, which depends on the instrument characteristics and performance (equation 6). In this section we show some of the outputs derived by applying the radiometric model to the three SIMBIO-SYS channels.

4.1.1 STC outputs

The transmission properties of all filters F(λ) and the detector quantum efficiency QE(λ) are taken from Da Deppo et al. (2016),[5] while the values of the telescope transmission T(λ) considered are a mean of 0.5 for the 420 nm filter, and almost trasparent for the other filters.

Figure 3 shows the expected signal in DN/ms for the broad-band (color) and PAN filters (left-side plots and right-side plots respectively) as function of the position of the S/C in its orbit around the planet, thus w.r.t. the bore-sight latitude. In this work we considered only the results obtained at aphelion ($\nu = 180°$), and we will present the complete results in future works.

As expected, the calculated signal for the two STC sub-channels, called H and L, which are looking forward and backward with respect to the nadir direction, reaches the maximum value for different positions of the S/C in its orbit. This effect is explained by the different values of radiance obtained for the two channels, which derives from the difference between the incident, emission and phase angle of the boresight of the two sub-channels.

A further important result showed in figure 3 is the consistent reduction of the maximum expected signal from the zero-latitude to the poles. This effect happens only when Mercury is near the aphelion. In this case the incidence, emission and phase angles sit on the same plane, so the phase is the sum of i and e. The consequence is that the phase angle greatly varies from the zero-latitude to the poles, and so that the Mercury reflectance. This situation is not expected for true anomaly different from the aphelion, because the MPO orbit is inertial. For $\nu \neq 180°$and $0°$ the three angles sit on different plane, so that the phase angle varies slightly with the latitude.

We compare our values derived for true anomaly $\simeq 180°$ and latitude zero with those obtained by Da Deppo et al. (2016). The expected signal obtained is 20% higher with respect to the previous estimate. The only exception is the 420 nm filter, for which our value is 30% lower. The difference between our values and the previous estimation can be explained by considering the differences in the estimation of the Mercury radiance, which depends on the reflectance model used. Another reason of the discrepance in the results can be ascribed to the different instrument and orbit configuration considered. Indeed, we take into account that the real S/C orbit is tilted, thus the periherm does not belong to equatorial plane. Furthermore, we take into account also the stereo configuration of the STC, while the nadiral direction has been considered by Da Deppo et al. (2016).

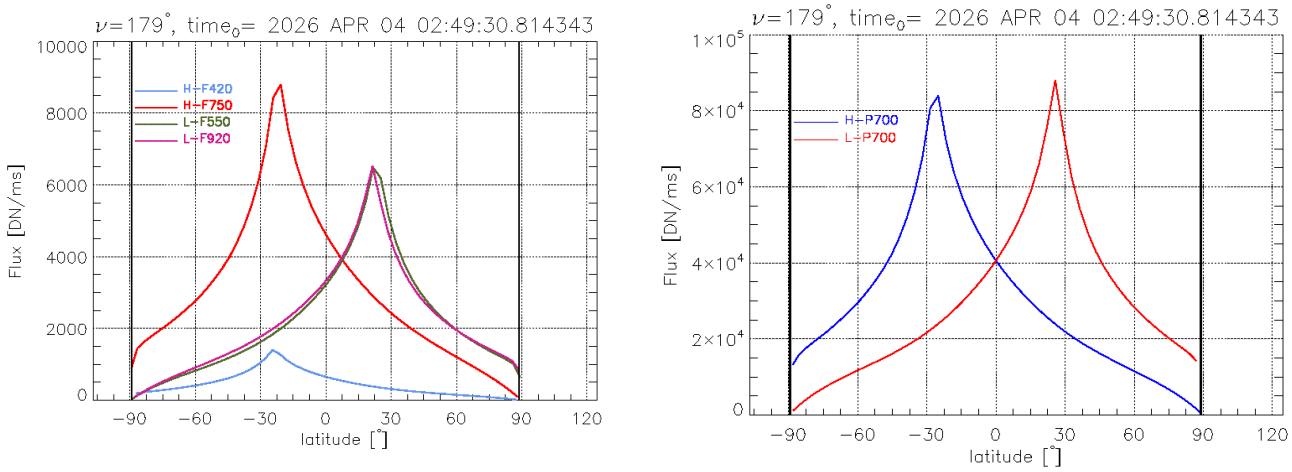

Figure 3. Expected Flux in DN/ms of color and PAN filters (left side and right side respectively) as a function of bore-sight latitude, for true anomaly 180°. The dark current measured in Leonardo at the nominal detector operating temperature T=268 K has been taken into account.

Another output obtained by our model is the expected best integration time (IT) in order to obtained a signal within the linearity range of the detector and thus avoiding the detector saturation. It is derived from the expected signal using as Full Well the nominal value 90000 e^-. The integration times obtained for each filter are represented in figure 4, for color and PAN filters respectively. Dashed colored lines in figure 4 show the integration at 1/4 px. The figure 4 shows that our results are underestimated of 30% with respect to Da Deppo et al. (2016).[5] The main reason is that we take into account the model of DC in the calculation of the expected integration time, which has not been considered in the preliminary estimations of Da Deppo et al. (2016).[5] The other differences are the same that explain the diversity in the expected signal.

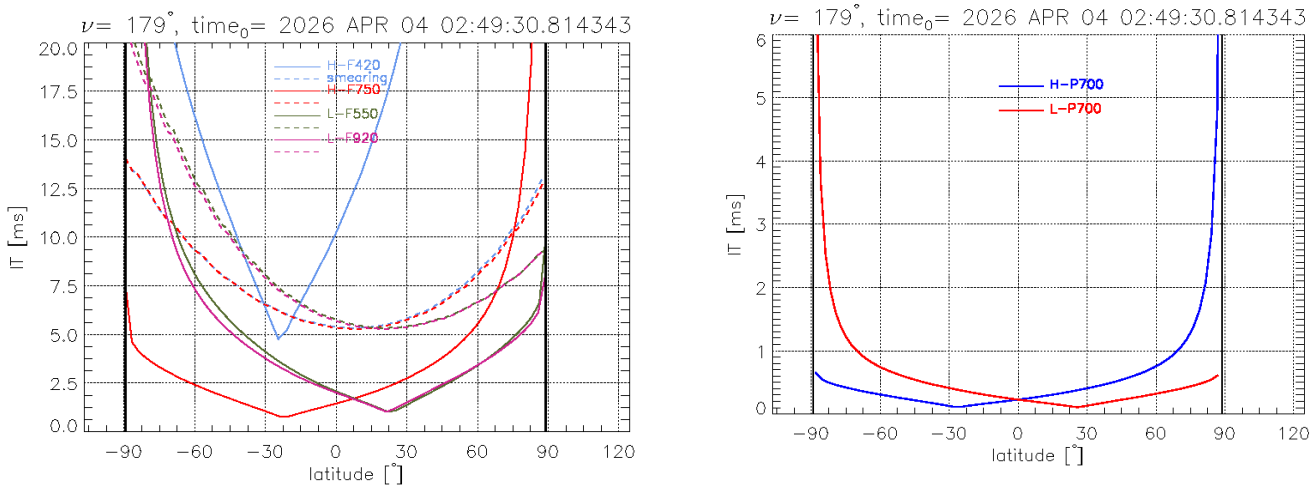

Figure 4. Best estimated integration time of color and PAN filters as a function of the bore-sight latitude, for $\nu = 180°$. The dash colored lines represent the calculate "smearing time" assuming a relative movement of 1/4 px. For PAN filters the smearing is not showed because it is out of the y-axis range. The contribution of the dark current (DC) measured at the nominal detector operating temperature (T=268 K) during the channel calibration campaign conducted at Leonardo S.p.A. has been taken into account to obtain the ITs.

The outputs of radiometric model allow some preliminary considerations about the instrument performance over the entire mission. Figure 5 shows the on-ground px dimension along track for two different values of the true anomaly in the first six months of observations. The figure shows that in both cases the on ground px dimension spans from ~ 56 m at periherm to ~ 112 m near the poles. The values of minimum and maximum px on-ground dimension vary slightly with the true anomaly values for the first six months of observations. This is not true for the last stages of the Bepicolombo mission, because of the variation of the argument of periherm and the minimum altitude with respect to the ground.

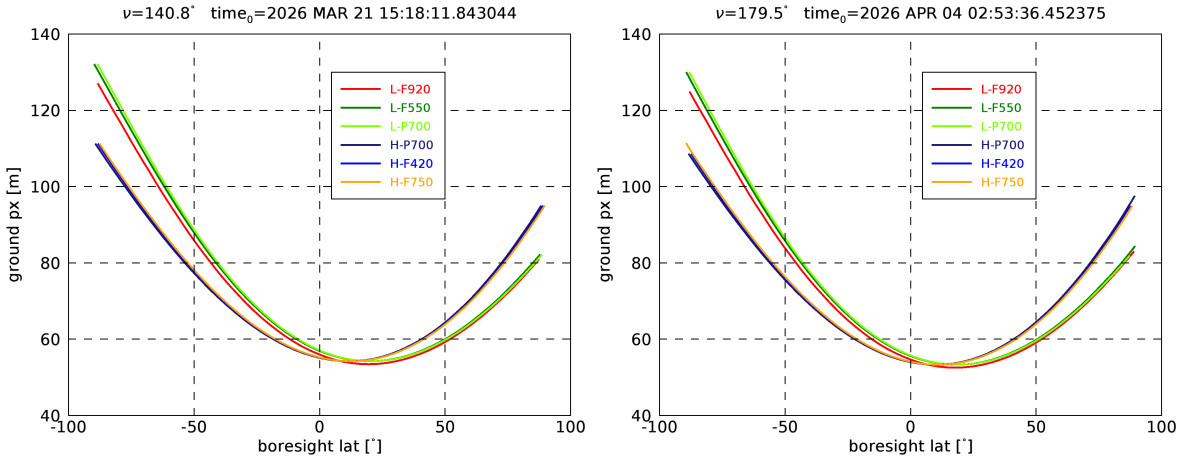

Figure 5. On ground px along track of STC as a function of the bore-sight latitude. The two plots are relative to two values of true anomaly.

4.1.2 HRIC outputs

The HRIC instrument properties are the transmission properties of the optical elementsT(λ), the filter transmissions F(λ), and the quantum efficiencies of the detector QE(λ). The measures of these quantities, as a function of the wavelength, has been provided by Leonardo S.p.A..

The Figure 6 includes a couple of plots that shows the estimation of flux in DN/ms for all the HRIC channel filters, as a function of the boresight latitude and for true anomaly $\nu = 180°$.

As expected, since the HRIC instrument observes in nadiral direction, the maximum value of flux is reached at latitude zero for all the HRIC filters, when the combination of incidence, emission and phase angles give the maximum reflectance. In the aphelion configuration, the incidence, emission and phase angles are located in the same plane, so that the phase angle is the algebraic sum of the incidence and emission angles. This fact implies that the phase angle varies greatly from the equator to poles, and then also the reflectance. The result is the great decreasing of the input flux from equator to the poles.

Despite the maximum radiance is obtained for zero latitude, the maximum on ground resolution of HRIC channel is obtained when MPO is at periherm. Figure 7 shows the on ground px dimension along track in the orbit as a function of the bore-sight latitude, for aphelion (left side plot) and perihelion (right side plot). The on ground px dimension varies from ~ 6 m at periherm to $\sim$ 13m near poles (left side panel). The different shape of the on-ground px dimension curve in the two plots has to be noticed. This effect is explained by considering the orbit of MPO: the peri-side arc covers the bright side of Merucry for the true anomaly interval $90° \leq \nu < 270°$, while for $270° \leq \nu < 360°$ and $0° \leq \nu < 90°$ the arc of the MPO orbit assigned to the observations is the apo-side.

Figure 8 shows the integration times as function of the bore-sight latitude for color and PAN filters. The true anomalies considered are the same of the Figure 6. The continuum line shows the integration times, while the dotted line is the smearing time calculated at 1/4 px.

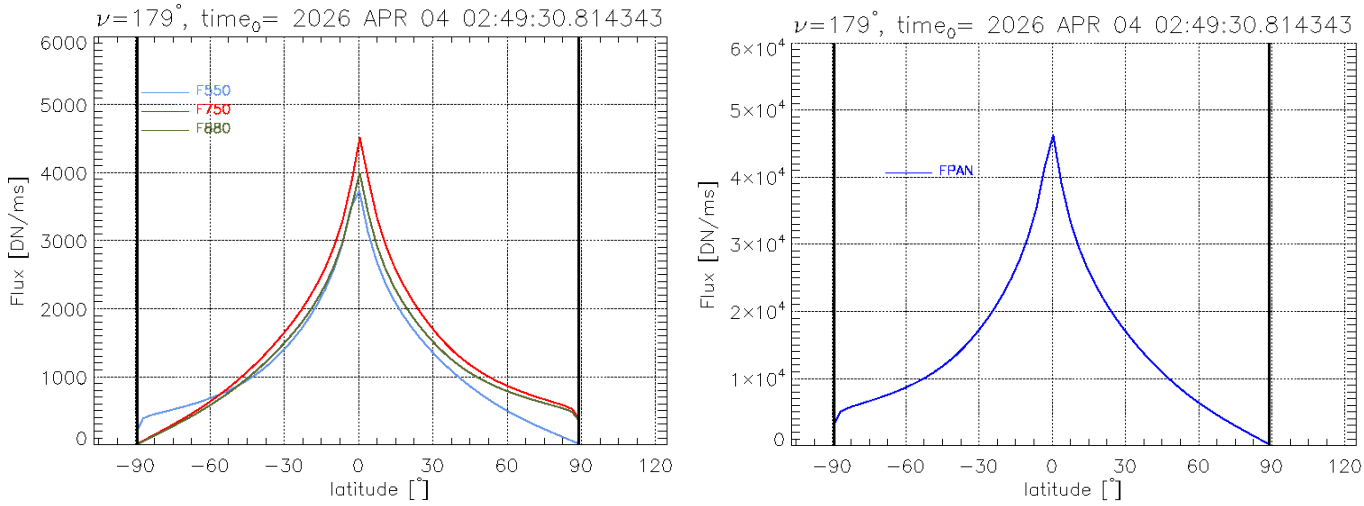

Figure 6. Flux in DN/ms expected for color filters (left-side column) and PAN filter (right-side column) of HRIC channel. All quantities are calculated as a function of the boresight latitude.

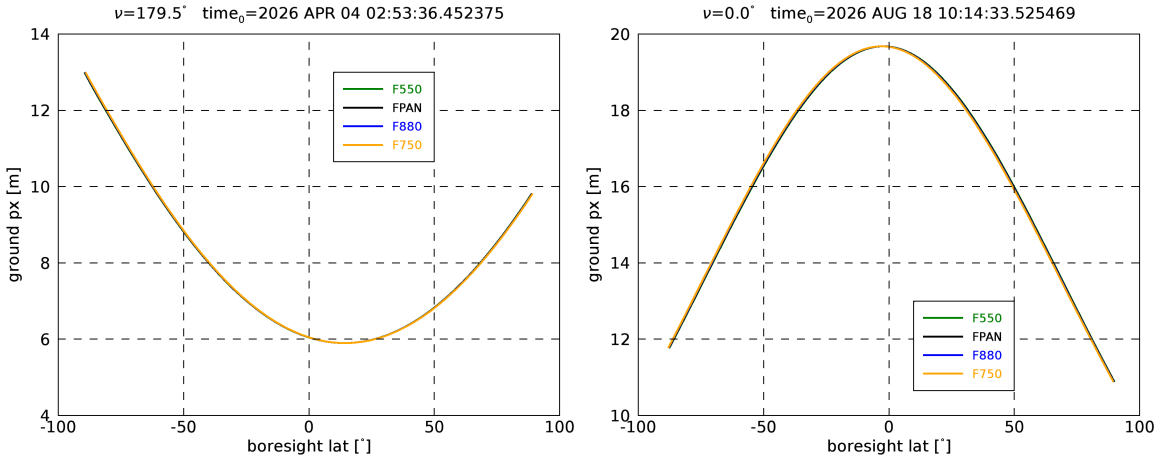

Figure 7. On ground px along track of HRIC as a function of the bore-sight latitude. The two plots are relative to two values of true anomaly.

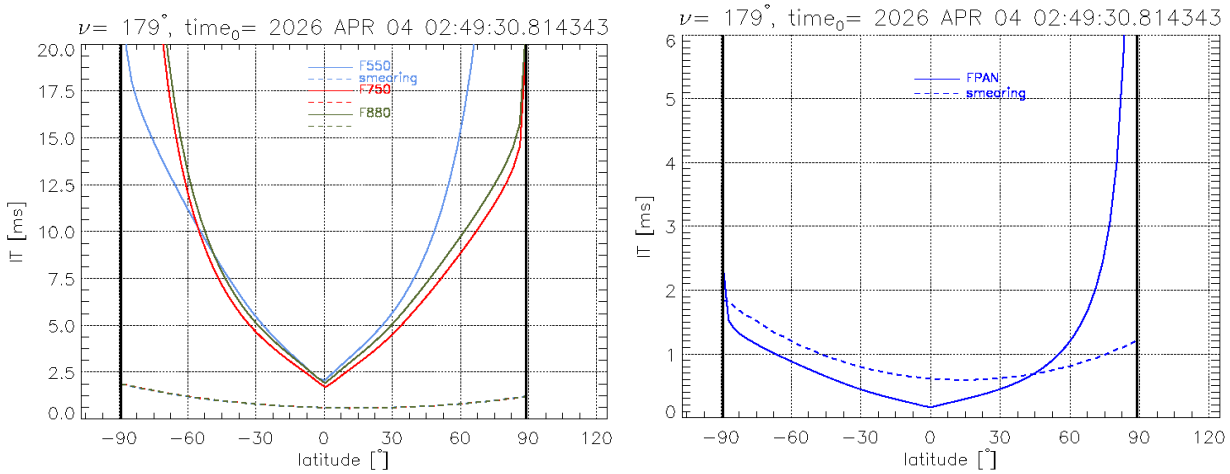

Figure 8. Integration time (continuum lines) and smearing (dashed lines) of HRIC channel, for color filter and PAN filter, as a function of bore-sight latitude. The results take into account the dark current measured by Leonardo S.p.A. during the on-ground detector calibration at the temperature of 268 K.

4.2 VIHI outputs

The VIHI channel resolves 256 spectral bands with a a spectral sampling of 6.25nm/band. Therefore, the calculation of the flux in DN/ms is obtained separately for each spectral band, using the equation:

$$F(\lambda_i) = \int_{\Delta\lambda} B(\lambda_i) \cdot \frac{1}{\pi} \cdot R(\lambda_i) \cdot \rho(\lambda_i) \cdot d\lambda_i \tag{7}$$

where $B(\lambda)[W/(\mu m \cdot m^2 \cdot sr)]$ is the sun spectrum obtained at the Mercury-Sun distance, $R(\lambda)$ is the reflectivity of the surface obtained with Hapke model, and the $\rho(\lambda)[DN \cdot \mu m \cdot m^2 \cdot sr/(W \cdot s)]$ is the instrument responsivity. The integral range $\Delta\lambda$ is 6.25 nm/band. Figure 9 shows the Flux in DN/ms obtained as function of the wavelength and the relative time with respect to the periherm (which is indicated as $time_0$). We shows the result for $\nu = 180°$ and $\nu = 0°$, relatives to the first six months of observations. From the comparison between the four plots we derive some considerations:

- The great variation of the flux detected with respect to the relative time is due to the peculiar configuration of the incidence, emission and phase angles described by the MPO orbit when Mercury is at aphelion and perihelion. This effect is the same described for HRIC and STC sub-channels. Furthermore, the weak difference observed between $\nu = 0°$ and $\nu = 180°$ is explained by considering that the MPO observes in the arc of the orbit that contains the apoherm and periherm, respectively.
- As expected, the maximum flux is estimated when MPO is near the latitude zero, when the incidence, emission and phase angles give the maximum reflectance.
- For all the true anomalies considered, the maximum flux corresponds to values of time different from zero. This effect can be explained considering that the apses line of MPO orbit is tilted with respect the equatorial plane, so that the the periherm do not coincides with the point of zero bore-sight latitude. The argument of the periherm is 16° at the beginning of the observations, and it decreases during the mission.

Once the flux in DN/ms has been obtained, it is possible to derive the integration times need to reach the full well capacity of the detector. The full well given by Raytheon Vision Systems is $2\,Me^-$, which corresponds to a saturation level of about 13200 DN after signal digitalization.[13] Figure 10 represents the integration times derived using the radiometric model, as a function of the wavelength and the relative time.

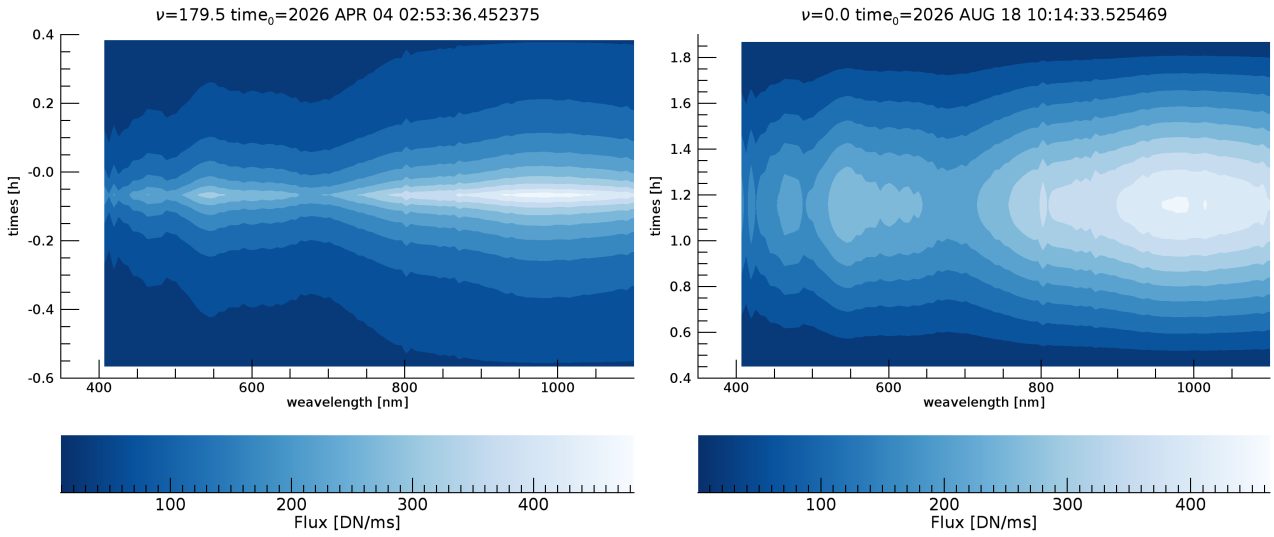

Figure 9. Flux of VIHI in DN/ms, as function of the relative time and the wavelength. Different plots shows the values obtained for different values of true anomaly.

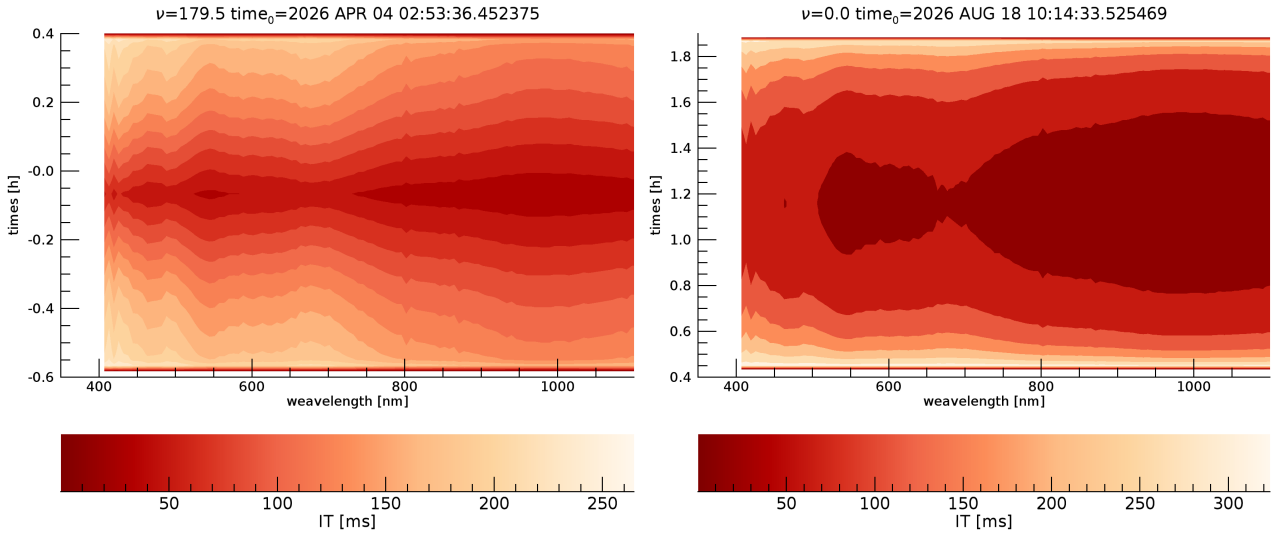

Figure 10. Flux of VIHI in DN/ms, as function of the relative time and the wavelength. Different plots shows the values obtained for different values of true anomaly.

5. CONCLUSIONS

In this work we have described the radiometric model of the Mercury surface and its application to the SIMBIO-SYS channels. Given the goal of the SIMBIO-SYS instrument to explore the Mercury surface in different wavelengths and with different spatial resolutions, the knowledge of the source radiance is necessary for each observed area. We obtain the Mercury surface reflectance using the Hapke parameters of Domingue et al. (2015)[11] and we derive the expected radiance for each point of Mercury surface. The result of Hapke reflectance model has been used as input parameter for the radiometric model.

The final result is a set of values which includes both the more generic information about the spacecraft motion (position and velocity), and the radiometric outputs valid for each SIMBIO-SYS channel, which are the values of radiance, the expected signal and integration times for each filter. These values are organized in tabels that refer to a specific true anomaly and absolute time, including the output for all filters and for the each instant of one S/C orbit around Mercury.

ACKNOWLEDGEMENTS

This activity has been realized under the BepiColombo Agenzia Spaziale Italiana (ASI) contracts to the Istituto Nazionale di Astrofisica (I/022/1070 and 2017-47-H.0) and with the support of Leonardo Company S.p.A. (Campi di Bisenzio (FI) – Italy).

REFERENCES

[1] Schulz, R. and Benkhoff, J., "BepiColombo: Payload and mission updates," *Advances in Space Research* **38**, 572–577 (Jan. 2006).

[2] Flamini, E., Capaccioni, F., Colangeli, L., Cremonese, G., Doressoundiram, A., Josset, J. L., Langevin, Y., Debei, S., Capria, M. T., de Sanctis, M. C., Marinangeli, L., Massironi, M., Mazzotta Epifani, E., Naletto, G., Palumbo, P., Eng, P., Roig, J. F., Caporali, A., da Deppo, V., Erard, S., Federico, C., Forni, O., Sgavetti, M., Filacchione, G., Giacomini, L., Marra, G., Martellato, E., Zusi, M., Cosi, M., Bettanini, C., Calamai, L., Zaccariotto, M., Tommasi, L., Dami, M., Ficai Veltroni, J., Poulet, F., Hello, Y., and Simbio-Sys Team, "SIMBIO-SYS: The spectrometer and imagers integrated observatory system for the BepiColombo planetary orbiter," *Lunar and Planetary Inst.* **58**, 125–143 (Jan. 2010).

[3] Re, C., Simioni, E., Cremonese, G., Roncella, R., Forlani, G., Da Deppo, V., and Naletto, G., "The first DTM generated by STC/SIMBIOSYS that will be on board the BepiColombo mission," in [*EGU General Assembly Conference Abstracts*], *EGU General Assembly Conference Abstracts* **17**, 15468 (Apr. 2015).

[4] Cremonese, G., Capria, M. T., Barbieri, C., Da Deppo, V., Fantinel, D., Forlani, G., Fornasier, S., Giro, E., Massironi, M., Naletto, G., Salemi, G., Sgavetti, M., Zaccariotto, M., Flamini, E., Debei, S., and SIMBIO-SYS international Team, "The stereo channel (STC) of the SIMBIO-SYS instrument for the BepiColombo mission to Mercury .," *Memorie della Societa Astronomica Italiana Supplementi* **9**, 173 (2006).

[5] Da Deppo, V., Martellato, E., Simioni, E., Naletto, G., and Cremonese, G., "Radiometric model for the stereo camera STC onboard the BepiColombo ESA mission," in [*Modeling, Systems Engineering, and Project Management for Astronomy VI*], *proc. SPIE* **9911**, 99111T (Aug. 2016).

[6] Mills, R. E., Drab, J. J., and Gin, A., "Advanced staring Si PIN visible sensor chip assembly for Bepi-Colombo mission to Mercury," in [*Astronomical and Space Optical Systems*], *proc. SPIE* **7439**, 74390A (Aug. 2009).

[7] Hapke, B. W., "Bidirectional reflectance spectroscopy. III. Correction for macroscopic roughness.," tech. rep. (1981).

[8] Hapke, B., "Bidirectional Reflectance Spectroscopy. 5. The Coherent Backscatter Opposition Effect and Anisotropic Scattering," *Icarus* **157**, 523–534 (June 2002).

[9] Hapke, B., Denevi, B., Sato, H., Braden, S., and Robinson, M., "The wavelength dependence of the lunar phase curve as seen by the Lunar Reconnaissance Orbiter wide-angle camera," *Journal of Geophysical Research (Planets)* **117**, E00H15 (Mar. 2012).

[10] Hapke, B., "Bidirectional reflectance spectroscopy 7. The single particle phase function hockey stick relation," *Icarus* **221**, 1079–1083 (Nov. 2012).

[11] Domingue, D. L., Murchie, S. L., Denevi, B. W., Ernst, C. M., and Chabot, N. L., "Mercury's global color mosaic: An update from MESSENGER's orbital observations," *Icarus* **257**, 477–488 (Sept. 2015).

[12] Domingue, D. L., Denevi, B. W., Murchie, S. L., and Hash, C. D., "Application of multiple photometric models to disk-resolved measurements of Mercury's surface: Insights into Mercury's regolith characteristics," *Icarus* **268**, 172–203 (Apr. 2016).

[13] Filacchione, G., Capaccioni, F., Altieri, F. Carli, C., Ficai Veltroni, I., Dami, M., Tommasi, L., Aroldi, G., Borrelli, D., and Barbis , A. Baroni, M. P. G., "The pre-launch characterization of for the BepiColombo mission to Mercury. II. Spectral calibrations," *Science Instruments* **88** (Sept. 2017).

[14] Blewett, D. T., Robinson, M. S., Denevi, B. W., Gillis-Davis, J. J., Head, J. W., Solomon, S. C., Holsclaw, G. M., and McClintock, W. E., "Multispectral images of Mercury from the first MESSENGER flyby: Analysis of global and regional color trends," *Earth and Planetary Science Letters* **285**, 272–282 (Aug. 2009).

[15] Denevi, B. W., Ernst, C. M., Prockter, L. M., Robinson, M. S., Spudis, P. D., Klima, R. L., Murchie, S. L., Solomon, S. C., Whitten, J. L., Povilaitis, R. Z., and Kinczyk, M. J., "The Origin of Mercury's Oldest Surfaces and the Nature of Intercrater Plains Resurfacing," in [*Lunar and Planetary Science Conference*], *Lunar and Planetary Inst. Technical Report* **47**, 1624 (Mar. 2016).

[16] Domingue, D. L., Murchie, S. L., Chabot, N. L., Denevi, B. W., and Vilas, F., "Mercury's spectrophotometric properties: Update from the Mercury Dual Imaging System observations during the third MESSENGER flyby," *Planet Space Sci.* **59**, 1853–1872 (Dec. 2011).

[17] Magrin, S., La Forgia, F., Da Deppo, V., Lazzarin, M., Bertini, I., Ferri, F., Pajola, M., Barbieri, M., Naletto, G., Barbieri, C., Tubiana, C., Küppers, M., Fornasier, S., Jorda, L., and Sierks, H., "Pre-hibernation performances of the OSIRIS cameras onboard the Rosetta spacecraft," *Astronomy and Astrophysics* **574**, A123 (Feb. 2015).

[18] Da Deppo, V., Naletto, G., Cremonese, G., and Calamai, L., "Optical design of the single-detector planetary stereo camera for the BepiColombo European Space Agency mission to Mercury," *App. Opt.* **49**, 2910 (May 2010).

[19] Head, J. W., Murchie, S. L., Prockter, L. M., Robinson, M. S., Solomon, S. C., Strom, R. G., Chapman, C. R., Watters, T. R., Blewett, D. T., Gillis-Davis, J. J., Denevi, B. W., Andre, S. L., Fassett, C. I., Dickson, J. L., Morgan, G. A., Kerber, L., Hurwitz, D. M., Ostrach, L. R., and MESSENGER Team, "Volcanism on Mercury: Characteristics and Distribution from the First MESSENGER Flyby," *AGU Fall Meeting Abstracts* , U11C–08 (Dec. 2008).

[20] Hawkins, S. E., Boldt, J. D., Darlington, E. H., Espiritu, R., Gold, R. E., Gotwols, B., Grey, M. P., Hash, C. D., Hayes, J. R., Jaskulek, S. E., Kardian, C. J., Keller, M. R., Malaret, E. R., Murchie, S. L., Murphy, P. K., Peacock, K., Prockter, L. M., Reiter, R. A., Robinson, M. S., Schaefer, E. D., Shelton, R. G., Sterner, R. E., Taylor, H. W., Watters, T. R., and Williams, B. D., "The Mercury Dual Imaging System on the MESSENGER Spacecraft," *Space science Rev.* **131**, 247–338 (Aug. 2007).

[21] Karimi, R., Ardalan, A. A., and Farahani, S. V., "Reference surfaces of the planet Mercury from MESSENGER," *Icarus* **264**, 239–245 (Jan. 2016).

[22] Lucchetti, A., Pajola, M., Cremonese, G., Carli, C., Marzo, G. A., and Roush, T., "Spectral Clustering on Mercury Hollows: The Dominici Crater Case," in [*Lunar and Planetary Science Conference*], *Lunar and Planetary Inst. Technical Report* **48**, 1329 (Mar. 2017).

[23] Murray, B. C., "The Mariner 10 pictures of Mercury - an overview," *Journal of geophysical research* **80**, 2342–2344 (June 1975).

[24] Solomon, S. C., "Mercury: the enigmatic innermost planet," *Earth and Planetary Science Letters* **216**, 441–455 (Dec. 2003).